RESOLUTION OF END-TO-END DISTANCE DISTRIBUTIONS OF FLEXIBLE MOLECULES USING QUENCHING-INDUCED VARIATIONS OF THE FORSTER DISTANCE FOR FLUORESCENCE ENERGY TRANSFER

IGNACY GRYCZYNSKI, WIESLAW WICZK, MICHAEL L. JOHNSON,* HERBERT C. CHEUNG,‡ CHIEN-KAO WANG,‡ AND JOSEPH R. LAKOWICZ
*University of Maryland at Baltimore, School of Medicine, Department of Biological Chemistry, Baltimore, Maryland 21201; *University of Virginia, School of Medicine, Department of Pharmacology, Charlottesville, Virginia 22908; and ‡University of Alabama at Birmingham, Department of Biochemistry, Birmingham, Alabama 35294*

ABSTRACT We describe a new method to recover the distribution of donor-to-acceptor (D-A) distances in flexible molecules using steady-state measurements of the efficiency of fluorescence energy transfer. The method depends upon changes in the Forster distance (R_0) induced by collisional quenching of the donor emission. The R_0-dependent transfer efficiencies are analyzed using nonlinear least squares to recover the mean D-A distance and the width of the distribution. The method was developed and tested using three synthetic D-A pairs, in which the chromophores were separated by alkyl chains of varying lengths. As an example application we also recovered the distribution of distances from the single tryptophan residue in troponin I (trp 158) to acceptor-labeled cysteine 133. The half-width of the distribution increases from 12 Å in the native state to 53 Å when unfolded by guanidine hydrochloride. For both TnI and the three model compounds the distance distributions recovered from the steady-state transfer efficiencies were in excellent agreement with the distributions recovered using the more sophisticated frequency-domain method (Lakowicz, J. R., M. L. Johnson, W. Wiczk, A. Bhat, and R. F. Steiner. 1987. *Chem. Phys. Lett.* 138:587–593). The method was found to be reliable and should be generally useful for studies of conformational distributions of macromolecules.

INTRODUCTION

Fluorescence energy transfer is widely used in the characterization of macromolecules, primarily to measure the distances between specifically labeled sites (1–4). These measurements are generally performed using steady-state methods, in which case it is generally necessary to assume the existence of a single distance between the donor (D)[1] and the acceptor (A). However, there are many instances in which a single D-A distance may not exist, such as between sites on a random coil polypeptide (4–6) or between lipids in cell membranes (7–13). In such cases the steady-state data can only yield a single apparent distance or demonstrate consistency of the data with a random distribution of D-A pairs. The steady-state transfer efficiencies measured with a single D-A pair or a single value of the Forster distance (R_0) cannot reveal the D-A distance distribution. Information on the distributions can be obtained from the time-resolved fluorescence data. Such distributions have been obtained using measurements of either the time-resolved decays of the donor (14, 15) or the frequency domain data (16, 17). However, such measurements require advanced instrumentation and analysis methods, resulting in limited availability to the biochemistry community.

In this report we describe a simple method to recover distance distributions using only steady-state measurements of the transfer efficiency. In 1971, Cantor and Pechukas (18) suggested that the macromolecule be labeled with several donors and several acceptors, so that the value of R_0 is varied over the widest possible range. Each D-A pair samples the distance distribution different-

Dr. Gryczynski was on leave from the University of Gdansk, Institute of Experimental Physics, Gdansk, Poland, with partial support from Central Project for Basic Research (CPBR) 01.06.2.01 (Poland), and Dr. Wiczk was on leave from the Department of Chemistry with partial support from CPBR 313.

[1] *Abbreviations used in this paper:* A, acceptor; D, donor; dansyl, 5-dimethylaminonaphthylene-1-sulfonyl; DTT, dithiothreitol; GuHCl, guanidine hydrochloride; hw, half-width, full-width of the Gaussian at the half-maximum intensity; IE, *N*-(iodoacetyl)-*N'*-(1-sulfo-5-naphthyl) ethylenediamine; IE-TnC, IE-labeled TnC; R_0, Forster distance; TCD, *N*-dansyl caproyl tryptamide; TnI, troponin I; tryptamine, 3-(2-aminoethyl)indole; TUD, *N*-dansyl undecanoyl tryptamide; TU2D, *N*-dansyl undecanoyl undecanoyltryptamide.

ly, and the transfer efficiencies measured using a number of D-A pairs should provide an estimate of the D-A distribution. To the best of our knowledge this method has not been used, probably because of the difficulties of labeling the molecule of interest with the different D-A pairs.

We now describe a simpler method to obtain a range of Forster distances. Collisional quenching was used to decrease the quantum yield of the donor, which in turn decreases the value of R_o. This possibility was mentioned briefly by Cantor and Pechukas (18), but to the best of our knowledge has not been reduced to practice. Due to the dependence of R_o on the sixth root of the quantum yield it is not possible to achieve a large range of R_o values. However, the simulations and experimental results indicate that even a 20% range of R_o values can yield good estimates of the D-A distribution. The method was verified using three D-A pairs, each linked by flexible alkyl chains of varying lengths (Scheme I). Additionally, the method was applied to troponin I, in the native state and when unfolded by guanidine hydrochloride. The recovered D-A distributions were found to be essentially identical to those found using the higher resolution frequency-domain method (manuscript in preparation).

THEORY

The efficiency of energy transfer can be calculated from the relative intensities of the donor (I_D) and the donor-acceptor pair (I_{DA}),

$$E^o = 1 - \frac{I^o_{DA}}{I^o_D}. \tag{1}$$

The superscript o indicates the absence of collisional quenching. If the donor and acceptor are present at a fixed distance (r) then the distance can be calculated from the efficiency using

$$E^o = \frac{R_o^6}{R_o^6 + r^6}, \tag{2}$$

where R_o is the Forster distance (4). The value of R_o is calculated from the spectral properties of the chromophores,

$$R_o^6 = \frac{9{,}000\,(ln10)\,\kappa^2\,\phi^o_D}{128\pi^5 N\, n^4} \int_o^\infty F_D(\lambda)\,\epsilon_A(\lambda)\,\lambda^4\,d\lambda, \tag{3}$$

where κ^2 is the orientation factor, ϕ^o_D the quantum yield of the donor in the absence of the acceptor and quencher, n the refractive index, N is Avogadro's number, $F_D(\lambda)$ is the emission spectra of the donor area normalized to unity, $\epsilon_A(\lambda)$ is the absorption spectrum of the acceptor in units of M^{-1} cm^{-1}, and λ is the wavelength in nanometers. In our analyses we assume $\kappa^2 = 2/3$ due to the range of conformations, the possibility of rotational diffusion and the mixed polarization of the chromophores (19). If desired, limits can be set on κ^2 from steady-state and/or time-resolved anisotropy measurements (20).

It is evident from Eq. 3 that the Forster distance depends on the sixth root of the donor quantum yield. In general it should be possible to reduce ϕ_D by 50-fold, which will decrease R_o to 52% of the original value. At high concentrations of quencher the extent of quenching is often due to both static and dynamic phenomena. The static component probably arises from the probability that the fluorophore is adjacent to a quencher at the moment of excitation. We found that it is necessary to use the dynamic component of the quenching for calculation of the quantum yield and the Forster distance for the quenched donor (R^Q_o). In retrospect this seems reasonable because the statically quenched species (dark complexes) do not contribute to the emission. The dynamic quenching constant can be obtained from measurements of the decay times, or from the dependence of the apparent quenching constant on quencher concentration. In the presence of both static and dynamic quenching the value of I^o_D/I_D is given by (21)

$$\frac{I^o_D}{I_D} = (1 + K_D[Q])(1 + K_S[Q]) \tag{4}$$

$$= 1 + (K_D + K_S)\,[Q] + K_D K_S\,[Q]^2, \tag{5}$$

where I^o_D and I_D are the donor intensities in the absence and presence of quencher, respectively, K_D and K_S are the dynamic and static quenching constants, and $[Q]$ is the quencher concentration. The apparent quenching constant is given by

$$K_{app} = \frac{I^o_D/I_D - 1}{[Q]}. \tag{6}$$

A plot of K_{app} vs. $[Q]$ is expected to be linear with a y-axis intercept of $K_S + K_D$ and a slope of $K_D K_S$. Solution of the

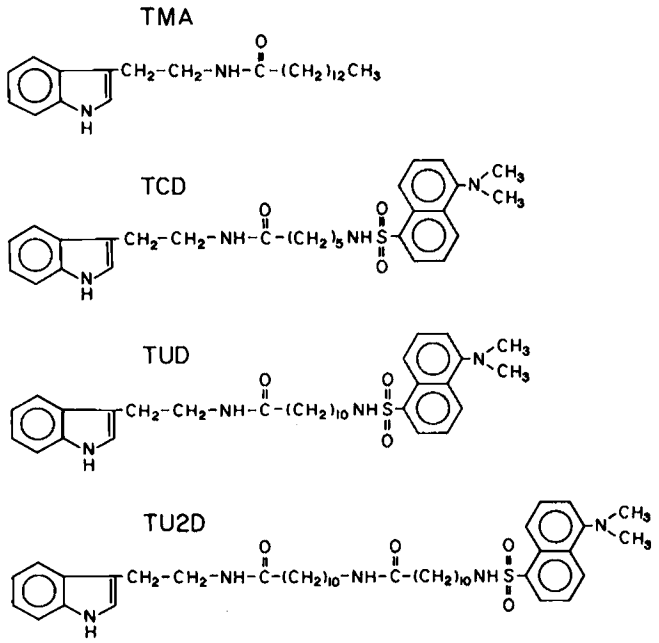

quadratic equation yields two values, and assignment of the correct value to K_D is accomplished either by decay time measurements or knowledge of the expected K_D values based on the quenching efficiency and/or solvent viscosity.

The quencher-dependent Forster distances (R_o^Q) are calculated from the decrease in quantum yield due to the collisional component of the quenching. In particular, the decrease in quantum yield due to collisional quenching is given by

$$\phi_D^Q = \frac{\phi_D^o}{1 + K_D [Q]}. \tag{7}$$

The quenched quantum yields are used to calculate the Forster distance using

$$R_o^Q = R_o \left(\frac{\phi_D^Q}{\phi_D^o}\right)^{1/6}. \tag{8}$$

The present data are probably not adequate to recover arbitrarily shaped distance distributions. To minimize the number of variable parameters, we assumed the D-A distributions to be described by a Gaussian.

$$P(r) = \frac{r^n}{\sigma \sqrt{2\pi}} \exp\left[-\frac{1}{2}\left(\frac{r - \bar{r}}{\sigma}\right)^2\right], \tag{9}$$

where $\bar{r}$ is the average, and σ the standard deviation of the distribution, and $n = 0$, 1, or 2. The standard deviation is related to the half-width hw (full-width at half-maximum) by hw = 2.354 σ. The parameters describing the D-A distribution were determined by nonlinear least squares (22). For any values of the assumed parameters the transfer efficiency can be predicted using

$$E_c^Q = \int_{r=r_m}^{\infty} \frac{P(r)(R_o^Q)^6}{(R_o^Q)^6 + r^6}\, dr, \tag{10}$$

where r_m is some minimum distance for the D-A pair. We found that the efficiency was not strongly dependent on the value of r_m, and we typically used r_m = 2 Å. The parameters describing the assumed distribution are varied to yield the minimum value of χ_R^2.

$$\chi_R^2 = \frac{1}{\nu} \sum_Q \left(\frac{E^Q - E_c^Q}{\Delta E}\right)^2 \tag{11}$$

where E^Q are the measured efficiencies at each R_o^Q value, ΔE = 0.01 is the estimated error in the measured efficiencies (E^Q), and ν is the number of degrees of freedom. The parameter values which yield the minimum value of χ_R^2 are taken to represent the D-A distribution of the experimental system.

At present the proper exponent for the distance in Eq. 9 is not known. For an infinite chain this exponent is probably 2, reflecting a three-dimensional volume element (23). For a rigid rod the correct exponent is probably zero. This point can only be clarified by further experimentation. Fortunately, the choice of n does not affect the visual appearance of the distance distributions.

MATERIALS AND METHODS

The synthetic donor-acceptor pairs are shown in Scheme I. The donor is the covalent adduct of tryptamine and myristic acid (TMA). There are three D-A pairs. In each case the donor is tryptamine, and the acceptor is dansyl (1-dimethylamino-5-naphthalenesulfonyl). The flexible spacer is either caproic acid (TCD), undecanoic acid (TUD), or a dimer of undecanoic acid (TU2D). The synthesis and purification of these compounds will be described elsewhere (19). The donor was excited at 295 nm, and its emission isolated with a 340-nm interference filter. It is important to avoid shorter excitation wavelengths, at which tyrosine residues might absorb light and transfer energy to the tryptophan residue. Magic angle polarization conditions were used to eliminate the effects of Brownian rotation. All solutions were in propylene glycol at 20°C. For calculation of R_o we used a refractive index of 1.4324. The quantum yield of the unquenched donor (TMA) was found to be 0.445, relative to a value of 0.13 for tryptophan in water (24). The quencher was acrylamide, which is known to be an efficient quencher of indole, tryptophan, and proteins (25).

TnI was isolated from rabbit skeletal muscle and purified as described previously (26). Cysteine 133 of TnI was labeled with *N*-(iodoacetyl)-*N'*-(1-sulfo-5-naphthyl)ethylenediamine as described by Wang and Cheung (27). The starting protein for labeling was troponin B (a complex formed between TnI and troponin C), in which the other two cysteine residues were inaccessible to sulfhydryl modification with iodoacetamide derivatives. The extent of modification was >98% as judged from sulfhydryl titration and the absorbance of the attached chromophore. As has been shown (27), the labeled TnI retained its ability to confer calcium sensitivity on reconstituted actosubfragment-1 ATPase, indicating that the label has a minimal effect on the conformation of TnI. The proteins were dissolved in 0.4 M KCl, 50 mM Tris, 1 mM EGTA, with 0.5 mM DTT, pH = 7.5 for all experiments except those involving GuHCl. In this case 5 M GuHCl replaced the 0.4 M KCl. All experiments were performed at 5°C using TnI concentrations near 35 μM. Forster distances from tryptophan 158 to IE-cysteine 133 were obtained from references 27 and 28.

The quencher acrylamide displays a weak absorption at the excitation wavelength. The apparent intensities (I_A) of the quenched samples were corrected for inner filter effects using

$$I_c = I_A\, 10^{OD/2}, \tag{12}$$

where OD is the optical density of the solution at the excitation wavelength and I_c is the corrected intensity. The experiments were performed in 3 × 10 mm path length cuvettes, with the 3-mm path length parallel to the direction of the excitation beam. The optical densities were measured in a 1 × 1 cm cuvette, and corrected for a path length of 3 mm for use in Eq. 12. Fluorescence decay times were obtained from the frequency response of the emission (29) using the 2 GHz harmonic-content instrument described previously (30). The decays were fit to a single or double exponential decay

$$I(t) = \sum \alpha_i\, e^{-t/\tau_i}, \tag{13}$$

where α_i are the preexponential factors and τ_i the associated decay times. The fractional intensity of each component in the decay is given by

$$f_i = \frac{\alpha_i \tau_i}{\sum \alpha_i \tau_i} \tag{14}$$

The mean decay times were calculated using

$$\langle \tau \rangle = \frac{\sum_{i=1}^{2} \alpha_i \tau_i^2}{\sum_{i=1}^{2} \alpha_i \tau_i}. \quad (15)$$

RESULTS

Simulations for Various D-A Distributions

Before presentation of the experimental results it is informative to examine the effects of changes in R_o^Q on the transfer efficiencies. These simulations reveal the effects of the distribution parameters ($\bar{r}$ and hw) on the extent of energy transfer. Additionally, least squares analysis of the simulated data, with added random noise, reveals the resolution that can be expected from the experimental data. Rather than describe a wide variety of simulations we chose to present selected examples which are comparable with the experimental results. Transfer efficiencies were calculated using Eq. 11, for both narrow (hw = 0) and wide (hw = 15 Å) Gaussians. The average distance ($\bar{r}$) was 10 or 20 Å, comparable with the value observed for the shortest (TCD) and the longest (TU2D) D-A pairs. In all cases the transfer efficiency decreases as R_o^Q is decreased. However, the dependence of E^Q on R_o^Q is much greater for a single D-A distance (Fig. 1, hw = 0, curve *B*) than for a distribution of distances (Fig. 1, hw = 15, curve *A*). Relative to a single D-A distance, the transfer efficiency for the D-A distribution is smaller at the higher values of R_o^Q. This is because some of the D-A pairs are extended, resulting in less energy transfer. Conversely, at the smaller R_o^Q values the transfer efficiency of the distributed D-A pair is higher because some of the donors and acceptors are closely spaced, permitting transfer even for small values of the Forster distance.

It is of interest to estimate the resolution of the distance

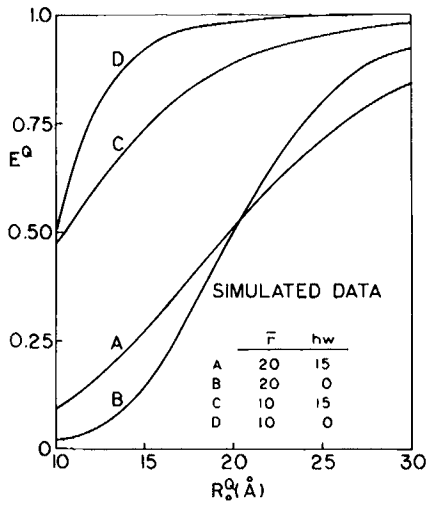

FIGURE 1 Simulated efficiency of fluorescence energy transfer for various donor-acceptor distance distributions.

distribution possible from the energy transfer data. We analyzed simulated data using two ranges of R_o^Q values. First we assumed R_o^Q could vary over the entire range shown in Fig. 1, that is, from 10 to 30 Å. This is clearly an optimistic case, in which the donor emission would be detected even after quenching a factor of $3^6 = 729$-fold. Secondly, we used R_o^Q values from 19 to 29 Å, which are closely comparable to our experimental data for the synthetic D-A pairs. For each assumed distribution we performed 20 separate simulations, each with different values for the random errors. The results of these simulations are summarized in Table I. Importantly, the recovered distributions agree with the simulated values, even for the more restricted range of R_o^Q values. Surprisingly, the standard deviations of the values recovered from the multiple simulations are quite small (0.05–1.0 Å), even for the narrow range of R_o^Q values. Somewhat larger standard deviations were found for an average distance of 10 Å. For this average distance the transfer efficiency is ~90% and varies little when R_o^Q is varied from 19 to 25 Å. Naturally, the resolution of $\bar{r}$ and hw is superior for the wider range of R_o^Q values. Importantly, the simulated data for the wide distributions cannot be fit with a narrow distribution. This is seen from the elevated values of χ_R^2 when the wide distribution E^Q values are force-fit with a narrow distribution. For instance, fitting of the data with $\bar{r} = 20$ and hw = 15 to a half-width of zero results in a 20-fold elevation of χ_R^2, even for the restricted 19–25 Å range of R_o^Q values. A larger elevation of χ_R^2 to 75.04 is found for the wider range of R_o^Q values. When the data are simulated for a narrow distribution the values of χ_R^2 are not changed when hw is held equal to zero during the analysis.

The resolution of $\bar{r}$ and hw expected from the data can also be predicted from examination of the χ_R^2 surface. These surfaces indicate the sensitivity of χ_R^2 to the values of $\bar{r}$ and hw. If the value of χ_R^2 is not sensitive to these parameters then one cannot expect to recover the parameters from the experimental data. We used a representative data set from the simulations in Table I. These data were analyzed with various fixed values of $\bar{r}$ and hw. The alternative parameter is permitted to vary so as to minimize the value of χ_R^2. As expected, the value of χ_R^2 is more strongly dependent on the parameters if the data extend from 10 to 30 Å (Fig. 2, *dashed lines*).

Nonetheless, χ_R^2 shows clear minima near the correct parameter values, even for the more limited range of R_o^Q values. This indicates that the data for this range of R_o^Q values should be adequate to recover the distance distributions.

Experimental Determination of D–A Distance Distributions

Emission spectra of TU2D at various concentrations of acrylamide are shown in Fig. 3. The emission centered at 360 nm is from the indole donor, and that centered at 500 nm from the dansyl acceptor. The emission spectra are

TABLE I
RECOVERED DISTANCE DISTRIBUTION FOR SIMULATED DONOR-ACCEPTOR PAIRS

Simulated values*		Range of R_o values	Recovered values		Standard deviations‡		χ^2_R for	
$\bar{r}$	hw		$\bar{r}$	hw	$\bar{r}$	hw	hw = 0§	hw ≠ 0
Å	Å	Å	Å	Å	Å	Å		
20	0.1	10–30	19.98	0.47	0.04	0.68	1.14	1.15
20	0.1	19–25	20.00	0.50	0.04	0.95	1.15	1.16
20	15	10–30	19.98	15.02	0.09	0.43	75.04	0.97
20	15	19–25	20.00	14.92	0.11	0.97	23.23	1.12
10	0.1	10–30	9.97	0.66	0.08	0.67	1.21	1.22
10	0.1	19–25	10.08	0.20	0.19	0.79	1.10	1.11
10	15	10–30	9.99	15.07	0.26	0.66	68.31	1.05
10	15	19–25	10.04	14.68	1.16	2.14	3.42	1.07

*In each simulation 11 values of R_o^Q were used, spaced approximately equally over the range of R_o^Q values. ‡The recovered values and standard deviations were obtained from analysis of 20 separate simulations, each with different random noise values. In each case the random error was assumed to be in the transfer efficiency, and equal to 0.01. §The hw was held equal to 0 during the least-squares analysis.

shown relative to that of the donor (TMA) at the same concentration of acrylamide. That is, the intensity scale for TMA and TU2D at each acrylamide concentration is shown at the same sensitivity. The intensity of the donor (TMA) at each acrylamide concentration was normalized to unity. In this way the indole intensity from TU2D reflects the extent of energy transfer independent of the amount of acrylamide quenching. In the absence of acrylamide the transfer efficiency is ~75%, as seen from the intensity of 360 nm in TU2D, relative to TMA. As the acrylamide concentration is increased the transfer efficiency decreases, as seen from the relative increase in donor emission at the higher concentrations of acrylamide. This decrease in efficiencies was predicted in Fig. 1 for smaller values of R_o^Q. Similar results were found for TCD and TUD (not shown). The transfer efficiencies for a range of acrylamide concentrations are summarized in Table II. The numerical values are given to facilitate comparison of the experimental data with theories for chain folding (23). The values >1.2 M in acrylamide were found to be unreliable, possibly because of the large corrections required for absorption of acrylamide at the excitation wavelength. To calculate the R_o^Q values for each acrylamide concentration it is necessary to determine the dynamic component of the quenching. This was particularly important for the present samples because of the highly nonlinear Stern-Volmer plot (Fig. 4, *open circles*), even after correction for inner filtering by acrylamide (Fig. 4, *solid circles*). We initially attempted to recover the D-A distribution using the corrected I_D^o/I_D values from Fig. 4, *solid circles*. The recovered distributions were not reasonable and did not agree with the frequency domain results on the same samples (manuscript in preparation and reference 16).

The dynamic component of the quenching was initially estimated using decay time measurements. The single and double exponential fits to the frequency response of the emission are summarized in Table III. In the absence of acrylamide the decay is dominately a single exponential near 6.5 ns, as is seen from the modest value of χ^2_R for the single component fit and the small fractional amplitude of the minor component (<1%). The decay times decrease in the presence of acrylamide, and the decays also become

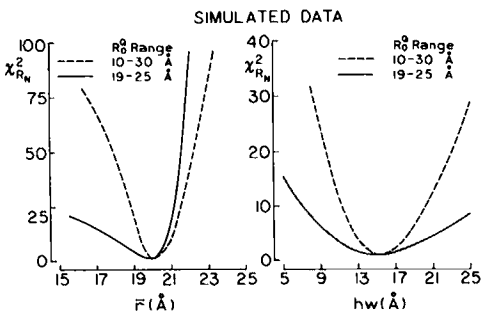

FIGURE 2 Dependence of χ^2_R on the values of $\bar{r}$ and hw. The simulated data were for 11 R_o values, spaced approximately equally over the range from 10 to 30 Å (*dashed lines*) or 19 to 25 Å (*solid lines*). R_o = 25 Å, $\bar{r}$ = 20 Å, and hw = 15 Å.

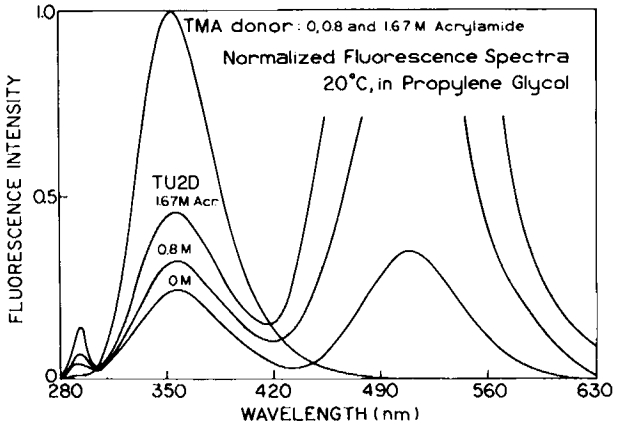

FIGURE 3 Emission spectra of TU2D with increasing concentrations of acrylamide. The amplitudes are adjusted so the donor intensity (TMA) is normalized at each acrylamide concentration.

TABLE II
TRANSFER EFFICIENCIES FOR TCD, TUD, AND TU2D

[Acrylamide]	R_o^*	Transfer efficiency for		
		TCD	TUD	TU2D
M	*Å*			
0	25.61	0.969	0.929	0.756
0.1	24.25	0.966	0.911	0.718
0.2	23.27	0.961	0.906	0.691
0.4	21.92	0.947	0.878	0.657
0.6	20.97	0.930	0.851	0.603
0.8	20.26	0.923	0.836	0.562
1.0	19.69	0.916	0.809	0.543
1.2	19.20	0.902	0.788	0.523

*Calculated using Eqs. 7 and 8 with $K_D = 3.85\ M^{-1}$.

considerably heterogeneous. This heterogeneity is known to be the result of transient effects in the mostly diffusion-controlled quenching reaction (31, 32). We plotted both the mean decay time, calculated from Eq. 14, and the decay time from the best single component fit to the data. These values of τ_D^o/τ_D indicate a dynamic quenching constant near 3.5 M^{-1}. The two quenching constants were determined separately by plotting K_{app} vs. $[Q]$, Fig. 5, yielding $K_1 = 3.85\ M^{-1}$ and $K_2 = 0.95\ M^{-1}$. By comparison with the decay time data we used $K_D = 3.85\ M^{-1}$ as the dynamic quenching constant. This value was used in Eqs. 7 and 8 to determine the quantum yield and R_o^Q value for each concentration of acrylamide (Table II).

The distance distributions were recovered from least

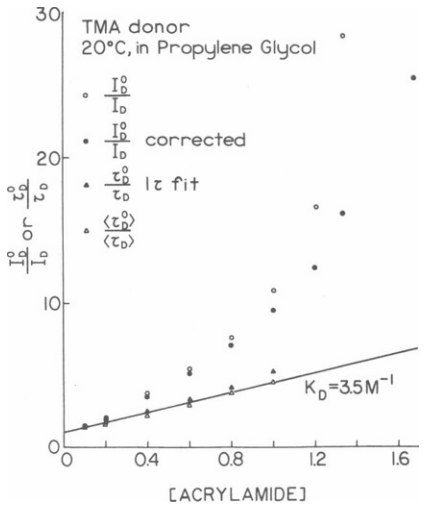

FIGURE 4 Stern-Volmer plot for acrylamide quenching of the donor (TMA). The values of I_D^o/I are shown corrected (*solid circles*) and not corrected (*open circles*) for inner filtering due to light absorption by acrylamide. Also shown are the decay time ratios for the best single exponential fits (*solid triangles*) and for the mean decay times (*open triangles*). The value of τ_D^o was 6.48 ns, and the mean decay time was calculated using $\langle\tau\rangle = \Sigma\ \alpha_i\ \tau_i^2/\Sigma\ \alpha_i\ \tau_i$, where α_i and τ_i are the preexponential factors and decay times recovered from a double exponential fit to the frequency domain data. The acrylamide concentrations refer to molarity.

TABLE III
DONOR DECAY PARAMETERS FOR TMA WITH INCREASING CONCENTRATIONS OF ACRYLAMIDE

[Acrylamide]	τ	$\langle\tau\rangle$	α_i	f_i	χ_R^2
M	*ns*	*ns*			
0	6.48	—	1.0	1.0	2.4
	0.38		0.048	0.003	
	6.54	6.53	0.952	0.997	1.2
0.2	4.03	—	1.0	1.0	53.5
	1.18		0.200	0.061	
	4.54	4.33	0.800	0.939	0.9
0.4	3.00	—	1.0	1.0	99.6
	0.79		0.265	0.075	
	3.52	3.32	0.735	0.935	1.0
0.6	2.24	—	1.0	1.0	143.1
	0.59		0.318	0.092	
	2.72	2.65	0.682	0.908	1.2
0.8	1.63	—	1.0	1.0	226.3
	0.39		0.436	0.125	
	2.13	1.90	0.564	0.875	1.7
1.0	1.27	—	1.0	1.0	278.4
	0.29		0.490	0.139	
	1.73	1.43	0.510	0.861	1.9

squares analysis of the transfer efficiencies. Comparison of the data and the calculated values are shown in Fig. 6, and one notices that the data are well approximated by the least squares fits with $\bar{r}$ and hw as floating parameters (*solid lines*). Importantly, the values of $\bar{r}$ and hw are in excellent agreement with frequency domain measurements on the same compounds (Table IV). The distributions recovered from the steady-state measurements (Fig. 6, *solid lines*) and from the frequency domain measurements (manuscript in preparation and reference 16) are shown graphically in Fig. 7, which again illustrates the good agreement between the distinct measurements. And finally, it should be noted that it was not possible to fit the data with narrow D-A distribution. This is seen from the mismatch between

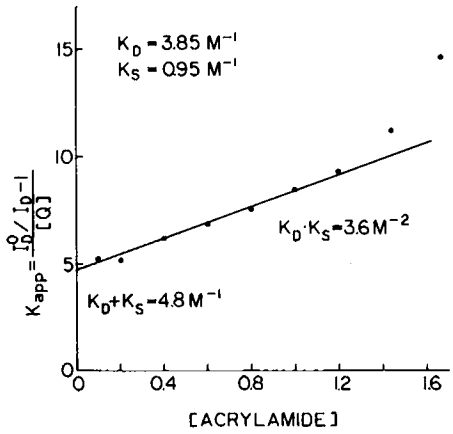

FIGURE 5 Determination of the static and dynamic quenching constants for TMA from the dependence of the apparent quenching constant on the acrylamide concentration. The acrylamide concentrations refer to molarity.

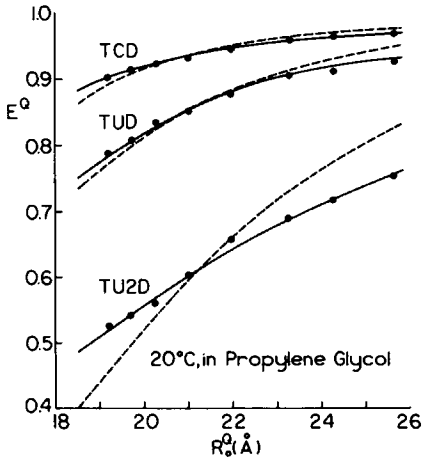

FIGURE 6 Least-squares fit of the transfer efficiencies to the values of R_o. From top to bottom the data are for TCD, TUD, and TU2D. In each case the symbols show the data, and solid lines show the best least squares fit to the data with variable values of $\bar{r}$ and hw (Table III). Dashed lines show the fits when the hw was held equal to 0.01 Å.

the measured data and the calculated curves for hw = 0.01 (Fig. 6), and from the elevated values of χ^2_R (Table IV).

We also examined the χ^2_R surfaces for the average distance and half-width for each of the compounds. These surfaces show considerable sensitivity to the values of $\bar{r}$ and hw. The greatest sensitivity of χ^2_R to $\bar{r}$ is shown by the data for TU2D (Fig. 8, *top*). This is probably because the values of R_o^Q for TU2D show the best overlap with the distance distribution, and because the transfer efficiencies for TU2D show the greatest change for this compound (Fig. 6 and Table II). Smaller changes in E^Q were observed for TCD and TUD, and the χ^2_R surfaces are less sharply centered on the average distance. Consequently their distance distributions are recovered with less certainty. The χ^2_R surfaces for the half-widths are similar for the three D-A pairs (Fig. 8, *bottom*).

The increasing resolution of the data for the series TCD,

TABLE IV
DISTANCE DISTRIBUTION PARAMETERS RECOVERED FROM LEAST-SQUARES ANALYSIS OF THE TRANSFER EFFICIENCIES

Compound/method	$\bar{r}$	hw	χ^2_R
	Å	Å	
TCD/SS*	9.7	12.7	0.10
	13.4	⟨0.01⟩	0.42
TCD/FD‡	8.1	11.9	—
TUD/SS	13.4	11.8	0.37
	15.6	⟨0.01⟩	2.08
TUD/FD	11.8	14.6	—
TU2D/SS	18.9	16.5	0.85
	19.7	⟨0.01⟩	23.21
TU2D/FD	20.0	15.5	—

*From the present steady-state (SS) data with quenching. ‡From the frequency domain (FD) measurements of the donor decays (manuscript in preparation and reference 16).

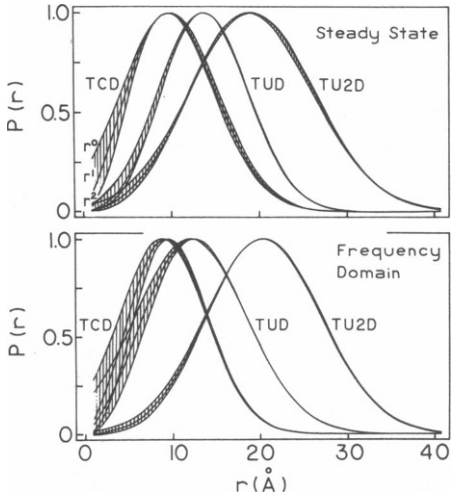

FIGURE 7 Distance distributions recovered for TCD, TUD, and TU2D. The curves are peak normalized. (*Top*) Distributions recovered from the present steady-state data. (*Bottom*) Distributions recovered from the frequency domain data (manuscript in preparation and reference 16). The multiple curves for each substance are the distributions found with r^0, r^1, or r^2 in Eq. 9.

TUD, and TU2D is also reflected in the values of χ^2_R for the fits obtained using a single distance (Table IV). We attempted to fit the data for each compound to a narrow (hw = 0.01) distribution. The values of χ^2_R are elevated for each substance, indicating the single distribution model is

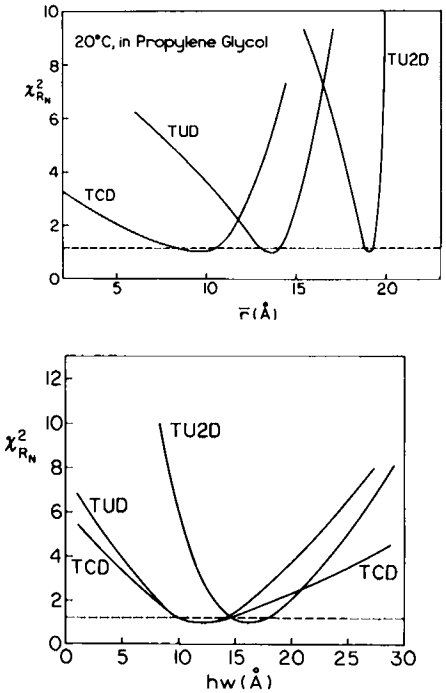

FIGURE 8 Dependence of χ^2_R on the average distance (*top*) and the half-width (*bottom*) for TCD, TUD, and TU2D. The value of $\bar{r}$ (hw) was held fixed at the value indicated on the *x*-axis, and the value of χ^2_R was minimized by variation in hw ($\bar{r}$). Dashed line shows the χ^2_R = 1.2, which should occur 37% of the time due to random errors in the data.

not adequate to account for the data. For the series TCD, TUD, and TU2D the values of χ^2_R for hw = 0.01 are elevated 4.2-, 5.6-, and 27.3-fold, respectively, indicating the higher distance information content for the energy transfer data centered near 50% transfer.

Distance Distributions in Native and Denatured Proteins

To further test our method we examined troponin I, in the native and random coil states. TnI contains a single tryptophan residue at position 158 which serves as the donor. The acceptor is provided by a covalently linked IE residue on cysteine 133. The specificity of labeling and Forster distances have been described previously (26–28). This system provided an ideal case because it contains a unique D-A pair. Secondly, the extent of energy transfer is 25% or less, which should test the resolution limits of the steady-state method. And finally, the distance distributions have already been determined using the frequency domain method (17), which allows comparison of the results.

Emission spectra of TnI and IE-TnI are shown in Fig. 9. The extent of energy transfer is modest. As expected, the extent of transfer decreases in 1 M acrylamide, which is the result of the decrease in the Forster distance.

Calculation of the R_o^Q values requires correction for static quenching. The static and dynamic quenching constants were separated using Eqs. 4–6. The value of K_D found from the plot agrees well with that found from the mean decay times (Fig. 10, *open triangles*). Similar experimental data were obtained for TnI in 6 M GuHCl, yielding quenching constants of $K_D = 4.35\ M^{-1}$ and $K_s = 0.40\ M^{-1}$ (not shown). In general it is not necessary to perform decay time measurements to obtain K_D, but we believe it is essential to plot K_{app} vs. $[Q]$. The initial slopes of the Stern-Volmer plots constructed from the corrected intensities do not yield reliable estimates of K_D.

Least squares fits of the transfer efficiencies (Table V) are shown in Fig. 11. The data (●) for native and denatured TnI are well fit by distributions with half-widths of 12.1 and 53.4 Å, respectively. The data could not be fit using

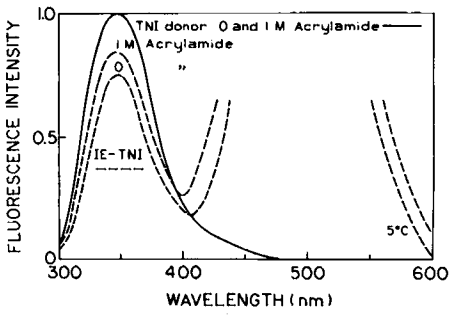

FIGURE 9 Emission spectra of TnI and IE-labeled TnI. The spectra of IE-TnI are shown relative to TnI at the same concentration of acrylamide.

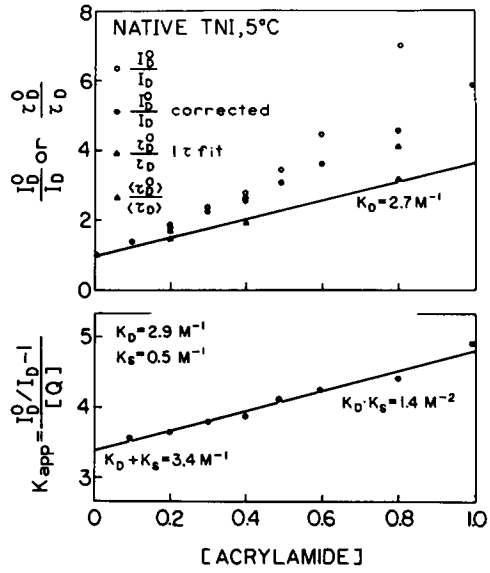

FIGURE 10 Stern-Volmer plot for acrylamide quenching of native TnI. For TnI in 6 M GuHCl (not shown) we found $K_D = 4.35\ M^{-1}$ and $K_S = 0.40\ M^{-1}$.

narrow distributions, as shown by the lack of overlap (Fig. 11) and by the elevated values of χ^2_R (Table VI). Importantly, the distributions recovered for native and denatured TnI are in excellent agreement with those found from the frequency-domain measurements (Fig. 12). As expected, the distribution of D-A distances is increased considerably in the random coil state.

And finally, we examined the χ^2_R surfaces to estimate the uncertainties in $\bar{r}$ and hw (Fig. 13). Relative to the synthetic D-A pairs the range of $\bar{r}$ and hw values consistent with the data is larger. Nonetheless, the ranges are not

TABLE V
TRANSFER EFFICIENCIES FOR NATIVE AND DENATURED IE-TnI AT 5°C

[Acrylamide]	Native*		Denatured‡	
	R_o^Q	E^Q	R_o^Q	E^Q
	Å		Å	
0	18.40	0.251	18.4	0.225
0.05	—		17.95	0.220
0.10	17.80	0.229	17.59	0.217
0.15	—		17.28	0.214
0.20	17.38	0.211	17.02	0.207
0.25	—		16.78	0.210
0.30	17.02	0.207	16.58	0.204
0.40	16.71	0.187	16.22	0.200
0.50	16.45	0.171	15.93	0.192
0.60	16.22	0.158	15.56	0.180
0.70	—		15.08	0.167
0.80	15.84	0.148	—	
0.90	—		14.77	0.164
1.00	15.52	0.137	—	

*Calculated using $R_o = 18.4$ Å and $K_D = 2.9\ M^{-1}$. ‡$R_o = 18.4$ Å and $K_D = 4.35\ M^{-1}$.

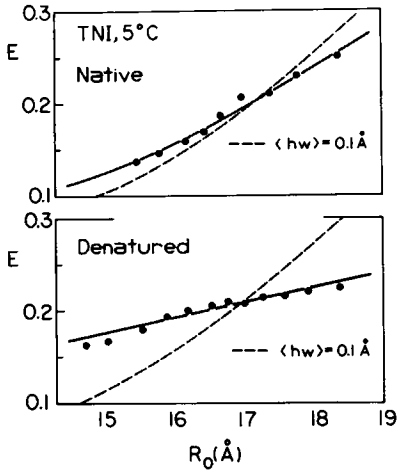

FIGURE 11 Least-squares fits of the IE-TnI energy transfer efficiencies. Data (*solid circles*) overlap with the values calculated for the distributions in Table VI, but do not overlap the values calculated for a narrow hw = 0.1 Å.

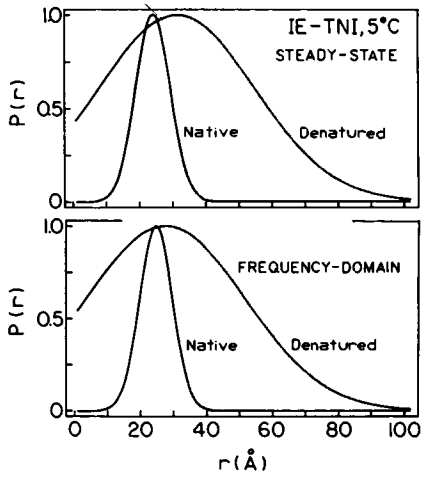

FIGURE 12 Comparison of the distance distributions for TnI recovered from the steady-state method (*top*) and the frequency domain measurements (*bottom*).

large, being 1–4 Å for $\bar{r}$ and 3–20 Å for hw. The larger range of 20 Å is primarily due to the small amount of energy transfer for denatured TnI at the larger distances.

DISCUSSION

The method described above provides the ability to recover the distribution of conformations for flexible molecules. Such measurements should be of widespread usefulness in the characterization of biological macromolecules. Multiple conformations are expected for many molecules, such as random coil peptides, single-stranded nucleic acids, and polysaccharides. Determination of the end-to-end distance distribution should allow comparison with calculated distribution based on assumed conformational potential functions. Additionally, this technique could be used to determine whether two sites on a structured macromolecule are in fact at a single distance, or whether there exist two or more distances as the result of multiple conformational states. The phenomenon of collisional quenching is rather general, with most fluorophores being quenched by one or more substances (33). Hence, the use of quenching-induced variations in the Forster distance can provide more detailed distance information from energy transfer studies, without the need for additional labeling of the macromolecules.

In recent years there has been an increased use of "global" analysis of distinct data sets to provide improved resolution of fluorescence spectral parameters. Global analysis has been applied to time (34) and frequency domain intensity (manuscript in preparation) and anisotropy decays (35). The ability to vary R_0 by quenching provides the opportunity for global analysis of the time and frequency domain data. These data may be obtained with different values of R_0, and each data set then provides a

TABLE VI
DISTANCE DISTRIBUTION IN IE-TnI RECOVERED FROM STEADY-STATE (SS) AND FREQUENCY DOMAIN (FD) MEASUREMENTS

Sample/method	$\bar{r}$	hw	χ^2_R
	Å	Å	
Native TnI/SS	23.8	12.1	0.3
	21.6	⟨0.1⟩	2.0
Native TnI/FD	23.0	12.0	0.9
	22.0	⟨1.0⟩	12.5
Denatured TnI/SS	30.8	53.4	0.2
	21.2	⟨0.1⟩	18.7
Denatured TnI/FD	27.0	46.9	0.8
	24.9	⟨1.0⟩	17.8

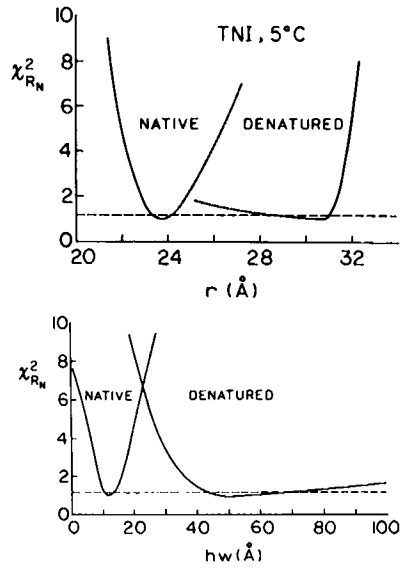

FIGURE 13 Dependence of χ^2_R on the values of $\bar{r}$ (*top*) and hw (*bottom*) for IE-TnI. The dashed line indicates the 67% confidence interval for the parameters.

different sampling of the D-to-A distribution. Simultaneous analysis of these data should provide an improved ability to recover the details of the D-to-A distance distribution.

The authors thank Professor Robert F. Steiner and Ms. Aneela Bhat for providing one of the donor-acceptor pairs.

Supported by grant GM-35154 from the National Institutes of Health, with support for instrumentation from the National Science Foundation (DMB-8511065 and DMB-8502835).

Received for publication 16 November 1987 and in final form 16 May 1988.

REFERENCES

1. Steinberg, I. Z. 1971. Long-range nonradiative transfer of electronic excitation energy in proteins and polypeptides. *Annu. Rev. Biochem.* 40:83–114.
2. Stryer, L. 1978. Fluorescence energy transfer as a spectroscopic ruler. *Annu. Rev. Biochem.* 47:819–846.
3. Lakowicz, J. R. 1983. Principles of Fluorescence Spectroscopy. Ch. 10. Plenum Publishing Corp., New York. 303–339.
4. Forster, T. 1948. Intermolecular energy migration and fluorescence. *Ann. Phys. (Leipzeig).* 2:55–75.
5. Haas, E., H. Wilchek, E. Katchalski-Katzir, and I. Z. Steinberg. 1975. Distribution of end-to-end distances of oligopeptides in solution as estimated by energy transfer. *Proc. Natl Acad. Sci. USA.* 72:1807–1811.
6. Amir, D., and E. Haas. 1986. Determination of intramolecular distance distributions in a globular protein by nonradiative excitation energy transfer measurements. *Biopolymers.* 25:235–240.
7. Fung, B. K. K., and L. Stryer. 1978. Surface density determination in membranes by fluorescence energy transfer. *Biochemistry.* 17:5241–5248.
8. Dewey, T. G., and G. G. Hammes. 1980. Calculation of fluorescence resonance energy transfer on surfaces. *Biophys. J.* 32:1023–1036.
9. Wolber, P. K., and B. S. Hudson. 1979. An analytical solution to the Forster energy transfer problem in two dimensions. *Biophys. J.* 28:197–210.
10. Estep, T. N., and T. E. Thompson. 1979. Energy transfer in lipid bilayers. *Biophys. J.* 26:195–208.
11. Shaklai, N., J. Yguerabide, and H. M. Ranney. 1977. Interaction of hemoglobin with red blood cell membranes as shown by a fluorescent chromophore. *Biochemistry.* 16:5588–5593.
12. Hauser, M., U. K. A. Klein, and U. Gosele. 1976. Extension of Forster's theory of long-range energy transfer to donor-acceptor pair in systems of molecular dimensions. *Z. Phys. Chem.* 101:255–266.
13. Davenport, L., R. E. Dale, R. H. Bisby, and R. B. Cundall. 1985. Transverse location of the fluorescent probe 1,6-diphenyl-1,3,5-hexatriene in model lipid bilayer membrane systems by resonance excitation energy transfer. *Biochemistry.* 24:4097–4108.
14. Haas, E., E. Katchalski-Katzir, and I. Z. Steinberg. 1978. Brownian motion of the ends of oligopeptide chains in solution as estimated by energy transfer between chain ends. *Biopolymers.* 17:11–31.
15. Katchalski-Katzir, E., and I. Z. Steinberg. 1981. Study of conformation and intramolecular motility of polypeptides in solution by a novel fluorescence method. *Ann. NY Acad. Sci.* 366:41–61.
16. Lakowicz, J. R., M. L. Johnson, W. Wiczk, A. Bhat, and R. F. Steiner. 1987. Resolution of a distribution of distances by fluorescence energy transfer and frequency-domain fluorometry. *Chem. Phys. Lett.* 138:587–593.
17. Lakowicz, J. R., I. Gryczynski, H. C. Cheung, C. K. Wang, and M. L. Johnson. 1988. Distance distributions in native and random coil troponin I from frequency-domain measurements of fluorescence energy transfer. *Biopolymers.* 27:821–830.
18. Cantor, C. R., and P. Pechukas. 1971. Determination of distance distribution functions by singlet-singlet energy transfer. *Proc. Natl. Acad. Sci. USA.* 68:2099–2101.
19. Haas, E., E. Katchalski-Katzir, and I. Z. Steinberg. 1978. Effect of orientation of donor and acceptor on the probability of energy transfer involving electronic transitions of mixed polarization. *Biochemistry.* 17:5064–5070.
20. Dale, R. E., J. Eisinger, and W. E. Blumberg. 1979. The orientational freedom of molecular probes. The orientation factor in intramolecular energy transfer. *Biophys. J.* 26:161–193.
21. Lakowicz, J. R. 1983. Principles of fluorescence spectroscopy. Plenum Publishing Corp., New York. 266–267.
22. Bevington, P. R. 1969. Data reduction and error analysis for physical sciences. McGraw-Hill Book Co., New York. 336 pp.
23. Flory, P. 1969. Statistical Mechanics of Chain Molecules. Academic Press, New York.
24. Chen, R. F. 1967. Fluorescence quantum yields of tryptophan and tyrosine. *Anal. Lett.* 1:35–42.
25. Eftink, M. R., and C. Ghiron. 1981. Fluorescence quenching studies with proteins. *Anal. Biochem.* 114:199–227.
26. Wang, C. K., and H. C. Cheung. 1985. Energetics of the binding of calcium and troponin I to troponin C from rabbit skeletal muscle. *Biophys. J.* 48:727–739.
27. Wang, C. K., and H. C. Cheung. 1986. Proximity relationship in the binary complex formed between Troponin I and Troponin C. *J. Mol. Biol.* 191:509–521.
28. Wang, C. K. 1985. Fluorescence studies of the interaction between Troponin I and Troponin C from rabbit skeletal muscle: energetics, intersubunit distances and anisotropy decays. Ph.D. thesis. University of Alabama at Birmingham.
29. Lakowicz, J. R., E. Gratton, G. Laczko, H. Cherek, and M. Limkeman. 1984. Analysis of fluorescence decay kinetics from variable-frequency phase shift and modulation data. *Biophys. J.* 46:463–477.
30. Lakowicz, J. R., G. Laczko, and I. Gryczynski. 1986. A 2 GHz frequency-domain fluorometer. *Rev. Sci. Instrum.* 57:2499–2506.
31. Joshi, N., M. L. Johnson, I. Gryczynski, and J. R. Lakowicz. 1987. Radiation boundary conditions in collisional quenching of fluorescence: determination by frequency-domain fluorometry. *Chem. Phys. Lett.* 135:200–207.
32. Lakowicz, J. R., M. L. Johnson, I. Gryczynski, N. Joshi, and G. Laczko. 1987. Transient effects in fluorescence quenching measured by 2-GHz frequency-domain fluorometry. *J. Phys. Chem.* 91:3277–3285.
33. Lakowicz, J. R. 1983. Principles of fluorescence spectroscopy. ch. 9. Plenum Publishing Corp., New York. 257–303.
34. Beechem, J. M., M. Ameloot, and L. Brand. 1985. Global analysis of fluorescence decay surfaces: excited state reactions. *Chem. Phys. Lett.* 120:466–472.
35. Gryczynski, I., H. Cherek, G. Laczko, and J. R. Lakowicz. 1987. Enhanced resolution of anisotropic rotational diffusion by multiwavelength frequency-domain fluorometry and global analysis. *Chem. Phys. Lett.* 135:193–199.